UNIVERSITY OF BIRMINGHAM
University of Birmingham Research at Birmingham

Near-tip strain ratchetting and crack growth at elevated temperature

Tong, J.; Cornet, C.; Lin, B.; Lupton, C.; Li, Hangyue; Bowen, P.; Williams, S.; Hardy, M.

DOI:
10.1016/j.ijfatigue.2015.09.006

License:
Creative Commons: Attribution-NonCommercial-NoDerivs (CC BY-NC-ND)

Document Version
Peer reviewed version

Citation for published version (Harvard):
Tong, J, Cornet, C, Lin, B, Lupton, C, Li, H, Bowen, P, Williams, S & Hardy, M 2016, 'Near-tip strain ratchetting and crack growth at elevated temperature', *International Journal of Fatigue*, vol. 82, no. Part 3, pp. 514-520. https://doi.org/10.1016/j.ijfatigue.2015.09.006

Link to publication on Research at Birmingham portal

General rights
Unless a licence is specified above, all rights (including copyright and moral rights) in this document are retained by the authors and/or the copyright holders. The express permission of the copyright holder must be obtained for any use of this material other than for purposes permitted by law.

•Users may freely distribute the URL that is used to identify this publication.
•Users may download and/or print one copy of the publication from the University of Birmingham research portal for the purpose of private study or non-commercial research.
•User may use extracts from the document in line with the concept of 'fair dealing' under the Copyright, Designs and Patents Act 1988 (?)
•Users may not further distribute the material nor use it for the purposes of commercial gain.

Where a licence is displayed above, please note the terms and conditions of the licence govern your use of this document.

When citing, please reference the published version.

Take down policy
While the University of Birmingham exercises care and attention in making items available there are rare occasions when an item has been uploaded in error or has been deemed to be commercially or otherwise sensitive.

If you believe that this is the case for this document, please contact UBIRA@lists.bham.ac.uk providing details and we will remove access to the work immediately and investigate.

Download date: 19. Apr. 2024

Accepted Manuscript

Near-Tip Strain Ratchetting and Crack Growth at Elevated Temperature

J. Tong, C. Cornet, B. Lin, C. Lupton, H.-Y. Li, P. Bowen, S. Williams, M. Hardy

PII: S0142-1123(15)00289-3
DOI: http://dx.doi.org/10.1016/j.ijfatigue.2015.09.006
Reference: JIJF 3713

To appear in: *International Journal of Fatigue*

Received Date: 27 March 2015
Revised Date: 1 September 2015
Accepted Date: 10 September 2015

Please cite this article as: Tong, J., Cornet, C., Lin, B., Lupton, C., Li, H.-Y., Bowen, P., Williams, S., Hardy, M., Near-Tip Strain Ratchetting and Crack Growth at Elevated Temperature, *International Journal of Fatigue* (2015), doi: http://dx.doi.org/10.1016/j.ijfatigue.2015.09.006

This is a PDF file of an unedited manuscript that has been accepted for publication. As a service to our customers we are providing this early version of the manuscript. The manuscript will undergo copyediting, typesetting, and review of the resulting proof before it is published in its final form. Please note that during the production process errors may be discovered which could affect the content, and all legal disclaimers that apply to the journal pertain.

ACCEPTED MANUSCRIPT

Near-Tip Strain Ratchetting and Crack Growth at Elevated Temperature

J. Tong*, C. Cornet, B. Lin, C. Lupton
Mechanical Behaviour of Materials Group, School of Engineering, University of Portsmouth, UK

H.-Y. Li, P. Bowen
University of Birmingham, UK

S. Williams, M. Hardy
Rolls-Royce plc, UK

ABSTRACT

In this work, we have extended our earlier work on the concept of ratchetting strain as a crack driving force (Tong *et al, Int J Fatigue,* 2014), to examine the crack growth of a nickel-based superalloy at selected temperatures in vacuum under both fatigue and fatigue-creep loading conditions. The parameters of a unified constitutive model were calibrated against the material data obtained at selected temperatures from 550 to 775°C, and a finite element model was developed to simulate the near-tip stress-strain responses under fatigue and creep-fatigue loading conditions at the experimental temperatures. Both ratchetting strain and accumulated inelastic strain near the crack tip were utilised in the prediction of the crack growth rates collected in vacuum. It seems that, although both ratchetting strain and accumulated inelastic strain correlate with the crack growth rates obtained under fatigue and fatigue-creep loading conditions, the predictions based on accumulated plastic strain are particularly close to the experimental results at all temperatures and loading conditions examined.

This is the first time the concept of ratchetting strain has been used to *predict* the crack growth rates of an engineering alloy at elevated temperature in vacuum, where the influence of oxidation on crack growth is removed.

KEYWORDS: Crack tip; viscoplasticity; ratchetting; accumulated inelastic strain; crack growth; elevated temperature; vacuum; nickel-based superalloy

1. Introduction

Considerable effort has been made towards an understanding of crack growth behaviour of nickel-based superalloys at elevated temperature under fatigue and fatigue-creep loading conditions, where creep, fatigue and oxidation may contribute concurrently to damage. Many studies [1-14] have been carried out on aspects of the subject, particularly the effects of loading variables [1–6, 10] and environment [7–10]. More recent published work concerns with the performance of a new generation of superalloys developed using powder metallurgy (PM) technique [6, 10]. The new alloys exhibit excellent creep resistance and high strength, but damage tolerance under fatigue and fatigue-creep loading conditions at increasing temperature remains a major challenge to fracture critical applications of these materials. More reliable life prediction approaches based on a fundamental understanding of the local events near a crack tip at elevated temperature are needed, hence research is essential to examine the crack growth behaviour in these new superalloys under typical operational conditions, and to explore the methods of characterisation of crack growth under these conditions.

Conventionally, crack growth rates at elevated temperature in nickel-based superalloys have been described based on a consideration of cycle-dependent and time-dependent regimes [14], sometimes with a third term considering creep-fatigue interaction [15]. This approach is phenomenological, and a separate treatment of cyclic plasticity (time-independent) and visco-plasticity (time-dependent) can be difficult, particularly in cases of creep-fatigue interaction prevailing in most high temperature applications. In this sense a unified approach that deals with viscoplasticity and cyclic plasticity as one inelasticity would seem advantageous. It is in this direction work has been carried out at Portsmouth on the constitutive modelling of viscoplastic behaviour of superalloys [16-20], where the

* Corresponding author: jie.tong@port.ac.uk; tel: +44 2392842326; fax: +44 2392842351

ACCEPTED MANUSCRIPT

unified Chaboche model was utilised [16,17] and modified [18, 19] to simulate fatigue, creep and fatigue-creep interaction in nickel-based superalloys. A damage parameter was also introduced [20] and used with some success for the description of damage evolution.

In 2004 we made an incidental discovery of ratchetting strain development near a crack tip, from a finite element analysis using a simple elastic-plastic constitutive model [21]. We found that, whilst the stress and the strain ranges remained essentially unchanged throughout the fatigue cycles and scaled with the external load range, progressive accumulation of tensile strains occurred near the crack tip. It became immediately clear that when the accumulated tensile strain reaches a critical value, material separation would occur. We have extended this work in recent years to consider viscoplastic material behaviour for growing cracks as well as stationery cracks of several materials and specimen geometries under a variety of loading conditions [22-24]. Again ratchetting behaviour was observed near the crack tip, which appears to be only weakly dependent of particular constitutive formulation and independent of specimen geometry. We successfully used the concept of critical ratchetting strain to predict the trends of crack growth under selected loading frequencies and dwell times for nickel-based alloys [22, 24]. Most recently, we have employed the digital image correlation (DIC) technique to measure, *in situ*, the normal strain evolution near a fatigue crack tip. Strain ratchetting was found by two independent experiments [25] for the first time. Although all the above work has been encouraging, we have yet to use the concept of ratchetting to predict experimentally measured crack growth rates at elevated temperature, due to the significant influence of oxidation on crack growth in air.

In this work, we have utilised the first set of crack growth data of a variant of alloy RR1000 collected in vacuum at selected temperatures to test the predictive capacity of the crack growth criteria based on the concept of strain ratchetting. To do so we have determined the materials parameters of the unified constitutive model [17] to cover a range of temperatures from 550 to 775°C. The predictive capability of the model for crack growth rates in vacuum has been tested at these temperatures and under fatigue and fatigue-creep loading conditions, with the effect of oxidation removed. This is the first time the concept of strain ratchetting is applied to the prediction of viscoplastic crack growth at elevated temperature.

2. The material model and parameter determination

2.1 The constitutive model

The material model is the Chaboche unified constitutive equations adopted by our group [17], where both isotropic and kinematic hardening variables are considered during the transient and the saturated stages of cyclic response without the consideration of plastic strain range memorisation. The model was available for isothermal conditions and the material parameters were available only for 650°C. To extend the model to include anisothermal conditions, we introduced a thermal strain to consider the influence of temperature [26]. This thermal strain component was added to the strain partitioning to represent the temperature dependency of the hardening components.

Within the small strain hypothesis and under uniaxial loadings, the total strain ε is partitioned additively into an elastic part ε^e, an inelastic part ε^p and a thermal strain ε^{th} :

$$\varepsilon = \varepsilon^e + \varepsilon^p + \varepsilon^{th} = \frac{\sigma}{E(T)} + \varepsilon^p + \alpha(T)\left(T - T_{ref}\right), \quad (1)$$

where $\alpha(T)$ is the thermal expansion coefficient dependent of temperature T.

The elastic strain rate $\dot{\varepsilon}^e$ obeys the Hooke's law:

$$\dot{\sigma} = E(T)\left(\dot{\epsilon} - \dot{\varepsilon}^p - \dot{\varepsilon}^{th}\right), \quad (2)$$

where E is the elastic modulus of the material and a function of temperature T.

ACCEPTED MANUSCRIPT

The inelastic strain $\dot{\varepsilon}^p$ represents both plastic and creep strains. A power-law relationship is adopted for viscous potential and inelastic strain rate is expressed as:

$$\dot{\varepsilon}^p = \left\langle \frac{f}{Z(T)} \right\rangle^{n(T)} \frac{\partial f}{\partial \sigma}, \tag{3}$$

where *f* is the yield function, *Z* and *n* are viscous parameters and functions of temperature *T*; and the sign function and the bracket are defined by:

$$sgn(x) = \begin{cases} 1, & x > 0, \\ 0, & x = 0, \\ -1, & x < 0, \end{cases} \quad \text{and} \quad \langle x \rangle = \begin{cases} x, & x \geq 0, \\ 0, & x < 0. \end{cases} \tag{4}$$

According to the von Mises yield criterion, the yield function *f* is defined as:

$$f(\sigma, \alpha, R, k) = J(\sigma - \alpha) - R - k(T) \leq 0, \tag{5}$$

where *R* is isotropic hardening variable, α is kinematic hardening variable, and *k(T)* is the initial value of the radius of the yield surface. The term *J* denotes the von Mises equivalent stress; for uniaxial case, it is expressed as:

$$J(\sigma - \alpha) = |\sigma - \alpha|. \tag{6}$$

The evolution of the kinematic stress α is described through the following rules [26]:

$$\begin{cases} \dot{\alpha} = \sum_{i=1}^{2} \dot{\alpha}_i \\ \dot{\alpha}_i = C_i(T) \left(\frac{2}{3} \alpha_i(T) \dot{\varepsilon}^p - \alpha_i \dot{p} \right) + \frac{\alpha_i}{C_i(T)\alpha_i(T)} \frac{\partial (C_i(T)\alpha_i(T))}{\partial T} \dot{T}, \end{cases} \tag{7}$$

where the kinematic hardening variable α is a summation of two components to describe the short and long range hardening, the parameters $C_i(T)$, $a_i(T)$ are material- and temperature- dependent constants. The thermal rate sensitivity of the model is also included. Under isothermal or bi-thermal conditions, this term vanishes and Equation 7 returns to the isothermal state.

The isotropic stress *R* is described as

$$\dot{R} = b(T)(Q(T) - R)\dot{p}, \tag{8}$$

where *b(T)* and *Q(T)* are material- and temperature- dependent constants which determine the shape and amplitude of the stress–strain loops during the transient and the saturated stages of cyclic response, and $\dot{p}$ is the accumulated inelastic strain rate defined by:

$$\dot{p} = |\dot{\varepsilon}^p| = \left\langle \frac{f}{Z(T)} \right\rangle^{n(T)} .. \tag{9}$$

ACCEPTED MANUSCRIPT

ACCEPTED MANUSCRIPT

The constitutive equations (1) to (9) contain a number of temperature dependent material parameters, namely, *E, k, b, Q, C_1, a_1, C_2, a_2, Z,* and *n*. For each kinematic hardening component α_i the saturated value is given by a_i while the value of C_i indicates the rate at which the saturated value is reached. The isotropic hardening *R* is depicted by *Q(T)* and *b(T)*, where *Q(T)* is the asymptotic value of *R* at saturation and b indicates the speed towards saturation. The initial size of the yield surface is represented as *k(T)*, and *E(T)* is the elastic modulus. These parameters were determined from the experimental data, obtained at selected temperatures from 550 to 775°C, in vacuum (3.1); and an optimisation procedure was used to obtain an optimum set of parameters based on a least-square method.

2.2 Parameter determination

At each temperature the full set of parameters was identified by a step-by-step procedure to obtain an initial set of parameters. These initial parameters were then used as the inputs in a simultaneous numerical routine for optimisation [17]. The basic experimental data including uniaxial cyclic stress-strain curves, stress relaxation and creep were used in an optimisation routine from which the optimised material parameters were obtained. The essence of this method is to seek a global minimum in the differences between the numerical and the experimental stress or strain. The difference between the values of stress/strain from the numerical analyses and the experiments is expressed as an objective function F:

$$F = \frac{1}{2}\sum_i^N \sum_j^M w_{ij}\left(Y_{ij}^{num} - Y_{ij}^{exp}\right)^2 \quad (10)$$

where Y_{ij}^{num} and $Y_{ij}^{\exp}$ represent the numerical and the experimentally measured stresses/strains respectively. N is the total number of experiments and M is the total number of the data points in the ith experiment. A weight factor w_{ij} was introduced to ensure equal contribution from each type of the experimental data, irrespective of the number of the data points in each experiment. A gradient-based Levenberg–Marquardt algorithm was used to obtain an optimum set of the material parameters. Global optimisation was carried out after the successful "staggered" optimisation of the grouped parameters. Penalty functions were introduced at each stage to ensure that the solutions were within the realistic physical and thermodynamic boundaries. Once all the parameters were optimised, a perturbation was made and the optimisation process was repeated until the optimised parameters were returned. Further details of the optimisation procedure are given elsewhere [18].

The model parameters were obtained in this manner for all of the temperatures of interest, and the optimised parameters are summarised in Figure 1.

2.3 Comparison of numerical simulation and experimental results

The optimised values of the parameters were then used in a FORTRAN program to simulate the cyclic behaviour of the material, and the simulated responses were compared with those obtained from the experiments. Good agreements were obtained at all temperatures. For clarity, only an example of the comparison between the numerical results and the experimental data is given here. Figure 2a shows the evolution of the first cycle of a simple strain-controlled cyclic test at a strain rate of 0.5%/s and a strain range of 3%. The test is fully reversed (strain ratio = -1) with a one second hold period introduced at both maximum and minimum loads. The comparison for the saturated cycle is shown in Figure 2b. Figure 2c

ACCEPTED MANUSCRIPT

represents the first cycle of a test at a strain rate of 0.5%/s, a strain range of 2% and a strain ratio of zero, where a 1 second hold period was introduced at both maximum and minimum loads. A comparison of the results of the saturated cycle is shown in Figure 2d. The simulations compare generally well with the experimental data for all cases. There is some overshoot in the transition from elastic to plastic during the first quarter of the cycle. But correction of this may require further up to three additional parameters [16], hence this was not attempted.

3. Crack growth prediction

The unified constitutive model [17] was adopted to predict the crack growth rates under baseline and selected dwell loading conditions at 550, 600, 650, 750 and 775°C, based on the model parameters obtained in (2.2), and the predicted results are compared with those collected from the experiments conducted in vacuum under the same loading conditions.

3.1 Experimental procedures

The crack growth rate data were generated in vacuum under constant amplitude cyclic loading with a load ratio of 0.1. Selected test temperatures were used ranging from 550 to 775℃. A corner crack test piece geometry with a cross section of 7×7 mm^2 was utilised, where a small notch of about 0.3 mm deep was introduced at one corner edge in the middle of the gauge section. The test pieces were precracked in vacuum at the test temperature under uniaxial tension fatigue loading at a frequency of 10 Hz. The crack growth tests were then carried out under a trapezoidal loading waveform: 1-X-1-1 (in second), where X = 1, 30, 300, 3600 (X = 1 represents a baseline test), to investigate the influence of dwell time on crack growth rate. A typical vacuum condition of ~2×10^{-5} mbar was achieved in all tests. A direct current potential difference (DCPD) technique was adopted to monitor automatically the crack growth. The crack lengths were verified post testing.

Under baseline cycling condition, the fracture mode was found to be predominantly transgranular; whereas ductile intergranular crack growth was observed at a combination of very high temperature and long dwell time, typically for dwell time over 30 second at temperatures of 750 and 775°C.

3.2 Finite element model

A plane strain finite element model of a single edge crack tension specimen was developed to simulate the crack growth in the diagonal (45°) direction of a 3D corner crack specimen used in the experiments (3.1). This specimen geometry was chosen to represent the worst-case scenario, also to reduce the computational costs of 3D simulation. The specimen was meshed into 4-nodded bilinear continuum plane strain elements, recommended for complex non-linear analyses involving severe element distortion around the crack tip (ABAQUS). The smallest element size at the crack tip was 12.7 μm. The crack length was chosen to be a = 3.5 mm and the ratio of crack length to specimen width, a/W, was 0.354. The finite element model and the detailed crack tip mesh are shown in Figure 3.

Simulation of crack tip deformation reveals distinctive strain ratchetting near the crack tip, leading to progressive accumulation of tensile strain normal to the crack growth plane, similar to those presented in [21-24]. We hypotheses that a crack starts to propagate when the ratchetting strain at a characteristic distance to the crack tip reaches a critical value. A ratchetting strain is the strain component perpendicular to the crack plane, $\varepsilon_{yy,}$ which coincides with the maximum principal strain. An accumulated inelastic strain, which is related to the ratchetting strain [22], was also used to correlate the crack growth rates. The accumulated inelastic strain was calculated by performing an integration of Equation (9) over time *t*:

ACCEPTED MANUSCRIPT

$$p = \int \left[\frac{f}{Z(T)}\right]^{n(T)} dt. \quad (11)$$

We utilised both ratchetting strain and accumulated inelastic strain in the prediction of the crack growth rates. Specifically, for a given stress intensity factor range, the number of cycles was recorded when the ratchetting strain or the accumulated plastic strain reached a critical value over a characteristic distance d^* = 12.7μm ahead of the crack tip. This critical value was then used to back calculate the crack growth rates at two other stress intensity factor values, below and above the current value, and the results were then compared those obtained experimentally. The details of the procedure were given elsewhere [22].

3.3 Results and discussion

Using both accumulated inelastic and ratchetting strains, the crack growth rates at 550, 600, 650, 750 and 775°C were predicted at selected values of ΔK in the mid-range of crack growth, and the results are compared with the experimental results obtained in vacuum. Figure 4 shows the comparison between the predictions and the experimental results. Encouragingly, both accumulated inelastic strain and ratcheting strain predict well the crack growth rates at the upper end temperatures 750 and 775C with long dwell periods (300s; 3600s), although the predicted slopes in the da/dN vs ΔK plots are somewhat slightly lower than those measured in the experiments. Predominantly creep influence may be at work under these conditions, which the unified model [16, 17] might not fully account for. At lower temperatures (up to 750C) and under baseline (1-1-1-1) or short dwell (30s) loading conditions, accumulated inelastic strain seems to correlate the crack growth rate data very well, whilst ratchetting strain over-predicts the slopes in the da/dN vs ΔK plots, although the general trends are not dissimilar. Ratchetting strain is a total strain at a given cycle, which is highly related to the accumulated inelastic strain at the same cycle. Although the initial elastic strain is contained in the ratchetting (total) strain, the subsequent elastic strains are largely recovered upon unloading/reloading, hence mainly inelastic strains remain in the ratchetting (total) strain after the first cycle. The two are almost identical when the inelastic strain is the predominant part, as shown in Figs 4 (h), (m), (n), under high temperature and long dwell loading conditions. When the elastic part is not negligible, the fatigue crack growth rates were over-predicted using the ratchetting (total) strain, whilst the accumulated inelastic strain predicted better (Figs 4(a) – 4(g)). This is possibly due to the formulation of the constitutive model, which is known to have a tendency of over-predicting ratchetting [23], hence faster crack growth rates. Nevertheless it is very encouraging that the concept seems to work for such a wide range of temperatures (600C-775C) and dwell periods (1s-3600s). The availability of the experimental results in vacuum is essential to remove the influence of oxidation, which is known to be considerable at elevated temperature. The viscoplastic deformation alone is responsible for the crack growth in the present work, which seems well quantified by the viscoplastic constitutive model.

Ratchetting deformation is known to have significant implications on material damage and fatigue life of components under service loading conditions. In our previous work, we have demonstrated that this phenomenon is not an artefact of the constitutive models used [23] or particular to specific materials or specimen geometries [24]. Rather, this is a physical phenomenon near a crack tip from our recent two independent experiments on stainless steel 316L [25]. In the present work, we have further demonstrated the predictive capacity of the concept for a number of crack growth cases of a nickel-based superalloy at elevated temperature, where the influence of oxidation is removed. Admittedly, the experimental data were collected from only one engineering alloy under selected loading conditions. Predictions were attempted based on the consideration of a characteristic length chosen mainly for convenience, and only limited simulations were run due to the computational costs. Furthermore, the ratchetting criterion is based on continuum mechanics principles, hence microstructure details are not

ACCEPTED MANUSCRIPT

considered. It must be said that crack growth mechanisms vary significantly, from predominantly intergranular under long dwell loading conditions at upper end of temperatures, to predominantly transgranular in baseline and short hold tests at lower temperatures. The fact that some cases are better predicted than the others may be indicative of the underline limitations in this approach. Ratchetting phenomenon has been found near *crack tips* in steels as well as alloys, hence we hypothesise that the concept might be applicable to crack growth in ductile metals, although further independent work is required to test this hypothesis. There may be materials in which no ratchetting occurs during cyclic loading, in that case Low Cycle Fatigue criterion should be used [27].

Further work is also needed to explore the relationship between a characteristic length and microstructure characteristics in both time-dependent and time-independent regimes. *In situ* experiments are being conducted to capture the strains at the onset of instantaneous crack growth with a view to formulating a crack driving force, efforts towards developing a physical-based model for crack growth under cyclic loading conditions.

4. Conclusions

a. A thermal strain component has been introduced in the unified Chaboche viscoplastic model to extend the unified Chaboche constitutive model to cover anisothermal conditions in the range of temperature from 600 to 775C. The optimised model parameters of a nickel-based superalloy are able to describe the experimental data very well.
b. The crack growth rate data of a nickel-based superalloy have been collected in vacuum under baseline and variable dwell (from 1s to 3600s) loading conditions at the selected temperatures from 600 to 775C.
c. A crack growth criterion based on the concept of ratchetting strain and accumulated inelastic strain has been utilised for the prediction of crack growth rates in vaccum. The predictions compare favourably with the experimental results, particularly at upper end temperatures 750 and 775, or using accumulated inelastic strain.

Acknowledgements:

The authors gratefully acknowledge the support from the Technology Strategy Board (TSB) of the UK as part of DEVELOPING IMPROVED SERVICE PROPAGATION LIVES IN ARDUOUS CYCLIC ENVIRONMENTS (DISPLACE) PROJECT, TP/8/MAT/6/I/Q1525K. We also thank Professor M Bache and Dr P Jones of the Swansea University who provided the test data at 750 and 775C with 30, 300, 3600 dwell periods.

5. References:

[1] Winston MR, Nikbin KM, Webster GA. Modes of failure under creep/fatigue loading of a nickel-based superalloy. J Mater Sci. 1985; 20:2471–6.
[2] Weerasooriya T. Effect of frequency on fatigue crack growth rate of Inconel 718 at high temperature. In: Fracture mechanics: nineteenth symposium, ASTM STP 969, 1988:907-23.
[3] Ghonem H, Nicholas T, Pineau A. Elevated temperature fatigue crack growth in alloy 718—part I: effects of mechanical variables. Fatigue Fract Eng Mater Struct 1993;16(5):565–76.
[4] Byrne J, Hall R, Grabowsk L. Elevated temperature crack growth in a nickel base superalloy. In: Behaviour of defects at high temperatures, ESIS 15, 1993:367-81.
[5] Lynch SP, Radtke TC, Wicks BJ, Byrnes RT. Fatigue crack growth in nickel-based superalloys at 500–700°C. I: Waspaloy. Fatigue Fract Eng Mater Struct 1994;17(3):297–311.
[6] Tong J, Byrne J. Effects of frequency on fatigue crack growth at elevated temperature. Fatigue Fract Eng Mater Struct1999; 22:185–93.

ACCEPTED MANUSCRIPT

ACCEPTED MANUSCRIPT
[7] Floreen S, Kane RH. An investigation of creep-fatigue environment interaction in a Ni-base superalloy. Fatigue Fract Eng Mater Struct 1980; 2:401–12.
[8] Gao M, Chen S-F, Chen GS, Wei RP. Environmentally enhanced crack growth in nickel-based alloy at elevated temperature. In: Elevated temperature effects on fatigue and fracture, ASTM STP1297, 1997:74–84.
[9] Bache MR, Evans WJ, Hardy MC. The effects of environment and loading waveform on fatigue crack growth in Inconel 718. Int J Fatigue 1999; 21:S69–77.
[10] Hide NJ, Henderson MB, Tucker A, Reed PAS. The effects of microstructure and environment on high temperature fatigue and creep-fatigue mechanisms in a nickel base superalloy. Prog Mech Behav Mater ICM8 1999;I.8:429–34.
[11] Barker VM, Johnson WS, Adair BS, Antolovich SD, Staroselsky A. Load and temperature interaction modeling of fatigue crack growth in a Ni-base superalloy. Int J Fatigue 2013; 52:95-105.
[12] Gustafsson D, Lundström E. High temperature fatigue crack growth behaviour of Inconel 718 under hold time and overload conditions. Int J Fatigue 2013; 48:178-86.
[13] Gustafsson D, Lundström E, Simonsson K. Modelling of high temperature fatigue crack growth in Inconel 718 under hold time conditions. Int J Fatigue 2013; 52:124-30.
[14] Jiang R, Everitt S, Lewandowski M, Gao N, Reed PAS. Grain size effects in a Ni-based turbine disc alloy in the time and cycle dependent crack growth regimes. Int J Fatigue 2014; 62:217-27.
[15] Liu H, Bao R, Zhang JY, Fei BJ. A creep-fatigue crack growth model containing temperature and interactive effects. Int J Fatigue 2014; 59:34-42.
[16] Tong J, Vermeulen B. The description of cyclic plasticity and viscoplasticity of Waspaloy using unified constitutive equations. Int J Fatigue 2003; 25:413-20.
[17] Tong J, Zhan ZL, Vermeulen B. Modelling of cyclic plasticity and viscoplasticity of a nickel-based alloy using Chabohe constitutive equations. Int J Fatigue 2004; 26:829-37.
[18] Zhan ZL, Tong J. A study of cyclic plasticity and viscoplasticity in a new nickel-based superalloy using unified constitutive equations. Part I: Evaluation and determination of the material parameters. Mech Mater 2007; 39:64-72.
[19] Zhan ZL, Tong J. A study of cyclic plasticity and viscoplasticity in a new nickel-based superalloy using unified constitutive equations. Part II: Simulation of cyclic stress relaxation. Mech Mater 2007; 39:73-80.
[20] Cornet C, Zhao LG, Tong J. A Study of Cyclic Behaviour of a Nickel-Based Superalloy at Elevated Temperature Using a Viscoplastic-Damage Model. Int J Fatigue 2011; 33:241-9.
[21] Zhao LG, Tong J, Byrne J. The evolution of the stress-strain fields near a fatigue crack tip and plasticity-induced crack closure revisited. Fatigue Fract Eng Mater Struct 2004;27:19-29.
[22] Zhao LG, Tong J. A viscoplastic study of crack-tip deformation and crack growth in a nickel-based superalloy at elevated temperature. J Mech Phys Solids 2008; 56:3363-78.
[23] Cornet C, Zhao LG, Tong J. Rachetting as a damage parameter for crack growth at elevated temperature. Eng Fract Mech 2009; 76:2538-53.
[24] Tong J, Zhao LG, Lin B. Ratchetting Strain as a Driving Force for Fatigue Crack Growth. Int J Fatigue 2013; 46:49-57.
[25] Tong J, Lin B, Lu YW, Madi K, Tai YH, Yates JR, Doquet V. Near-tip strain evolution under cyclic loading: In situ experimental observation and numerical modelling. Int J Fatigue 2015; 82:78–90.
[26] Yaguchi M, Yamamoto M, Ogata T. A viscoplastic constitutive model for nickel-base superalloy, part 2: modelling under anisothermal conditions. Int J Plast 2002; 18:1111-31.
[27] Kapoor A. A re-evaluation of the life to rupture of ductile metals by cyclic plastic strain. Fatigue and Fracture of Engineering Materials and Structures 1994; 17: 201–219.

ACCEPTED MANUSCRIPT

Figures:

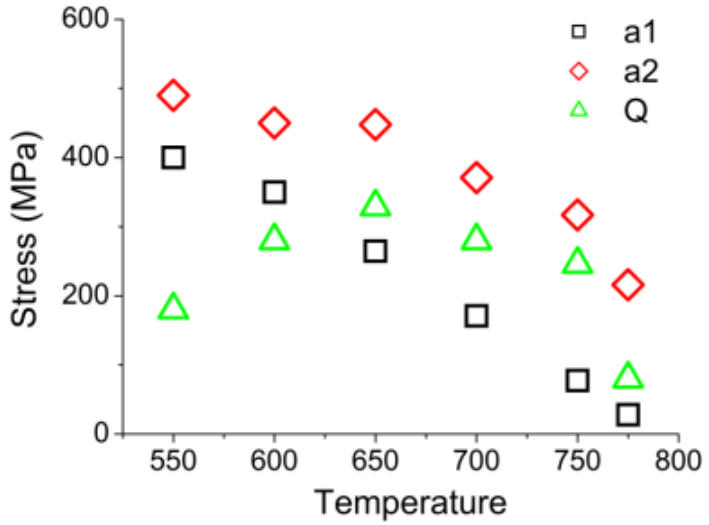

Figure 1a: Saturated values of the hardening parameters as a function of temperature.

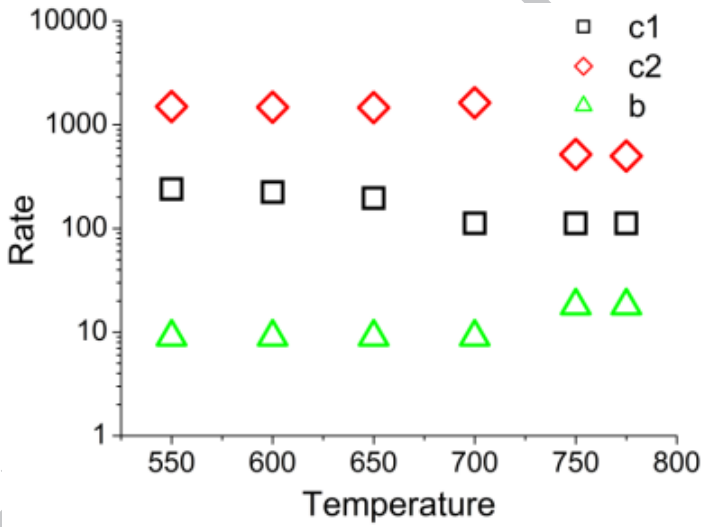

Figure 1b: Hardening rate parameters as a function of temperature.

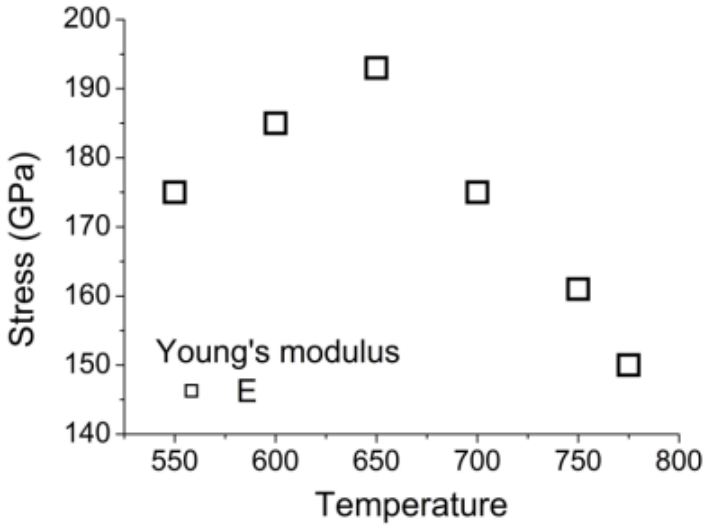

Figure 1c: Young's modulus as a function of temperature.

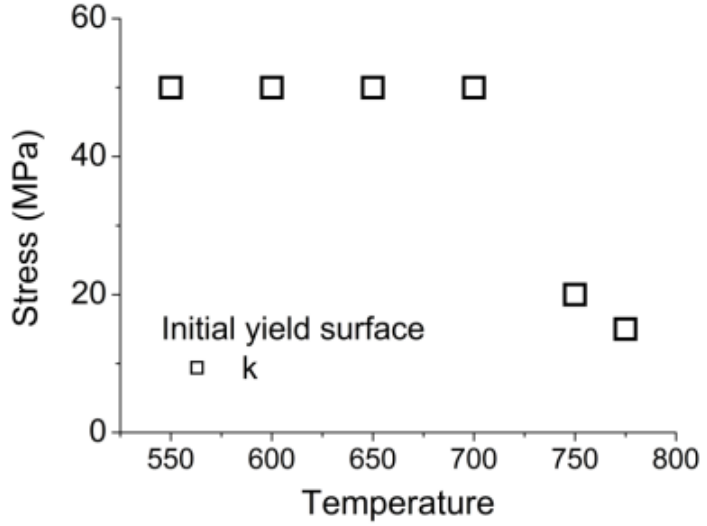

Figure 1d: Initial yield surface as a function of temperature.

ACCEPTED MANUSCRIPT

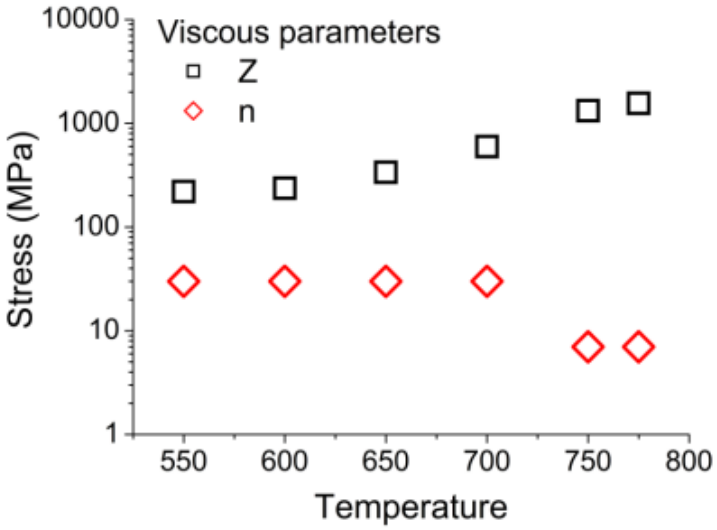

Figure 1e: The evolution of the viscous parameters as a function of temperature.

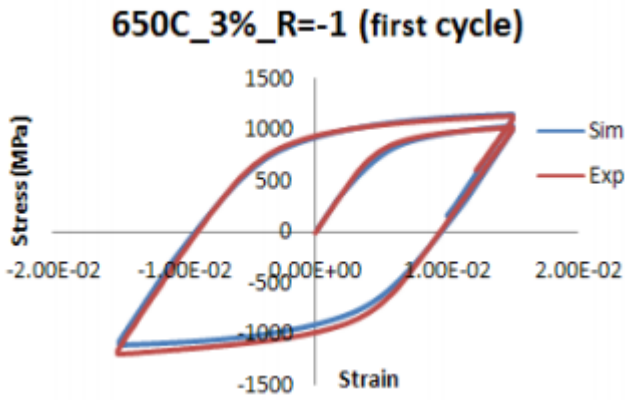

(a)

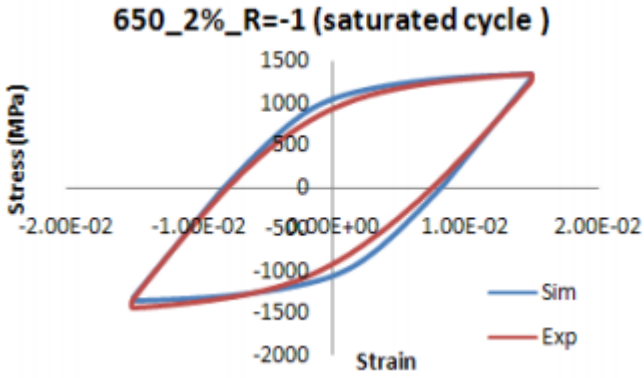

(b)

ACCEPTED MANUSCRIPT

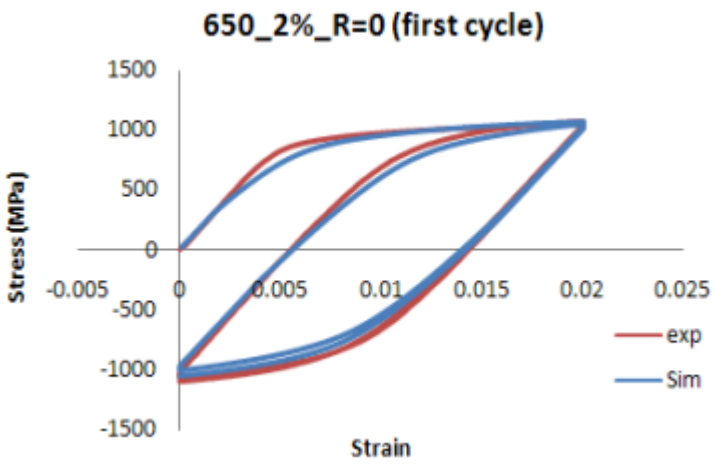

(c)

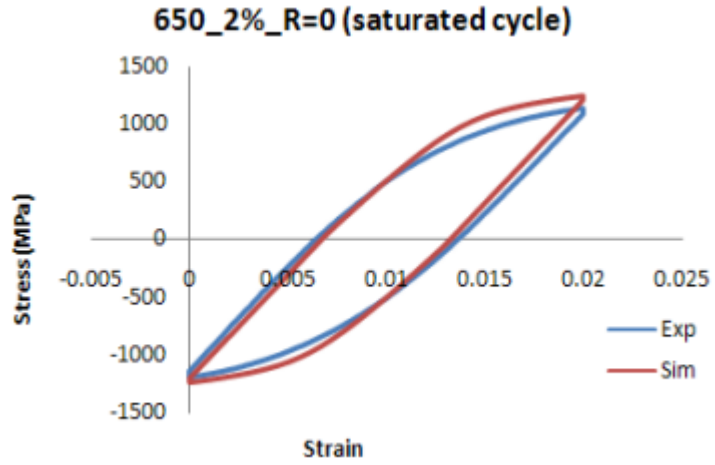

(d)

Figure 2: Comparison between the numerical simulation and the experimental results at 650C for (a) first cycle (strain rage Δε= 3%, strain rate έ=0.5%/sec, fully reversed with a dwell period of 1 sec at max/min loads); (b) saturated cycle with the same conditions as (a); (c) first cycle (strain rage Δε= 2%, strain rate έ=0.5%/sec, R = 0 with a dwell period of 1 sec at max/min loads); (d) saturated cycle with the same conditions as (c).

ACCEPTED MANUSCRIPT

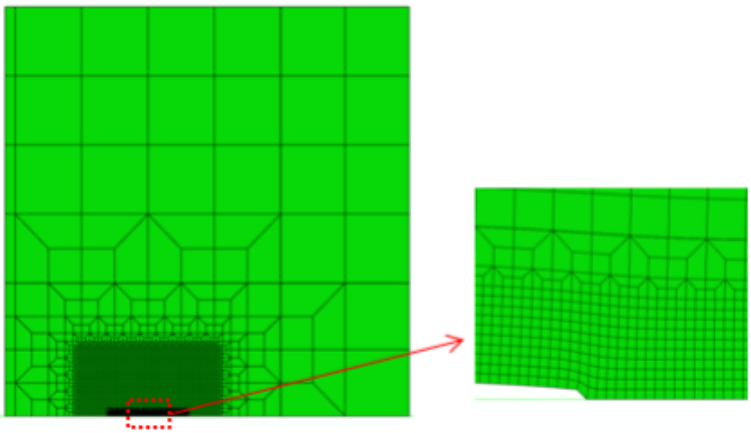

Figure 3: A plane strain finite element model of a single edge cracked tension (SECT) specimen.

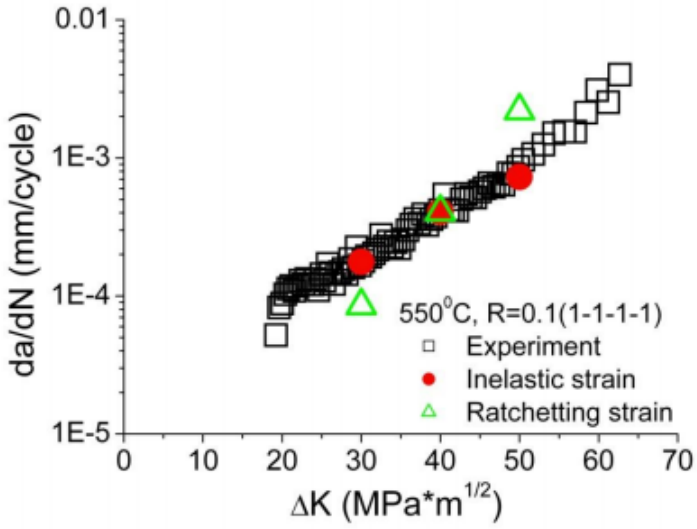

Figure 4 (a): Comparison of the results from the experiment and the FE model prediction for crack growth at 550°C (R=0.1; loading waveform 1-1-1-1).

ACCEPTED MANUSCRIPT

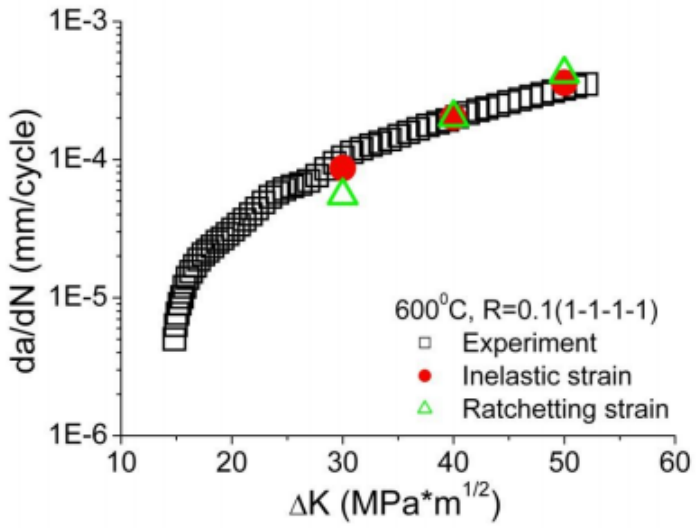

Figure 4(b): Comparison of the results from the experiment and the FE model prediction for crack growth at 600°C (R=0.1; loading waveform 1-1-1-1).

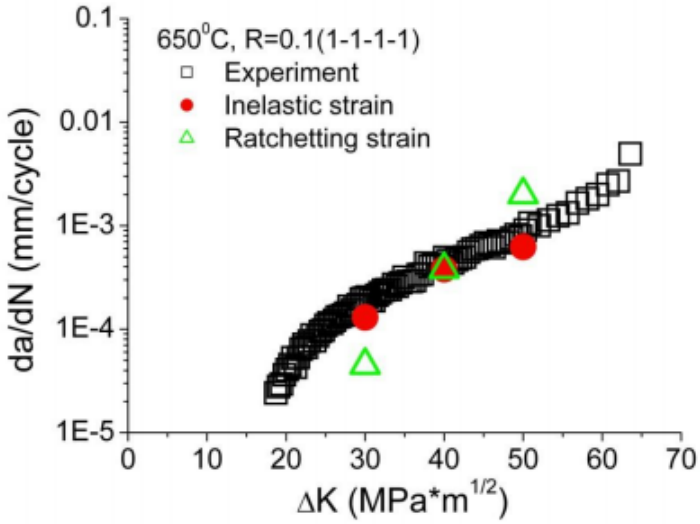

Figure 4(c): Comparison of the results from the experiment and the FE model prediction for crack growth at 650°C (R=0.1; loading waveform 1-1-1-1).

ACCEPTED MANUSCRIPT

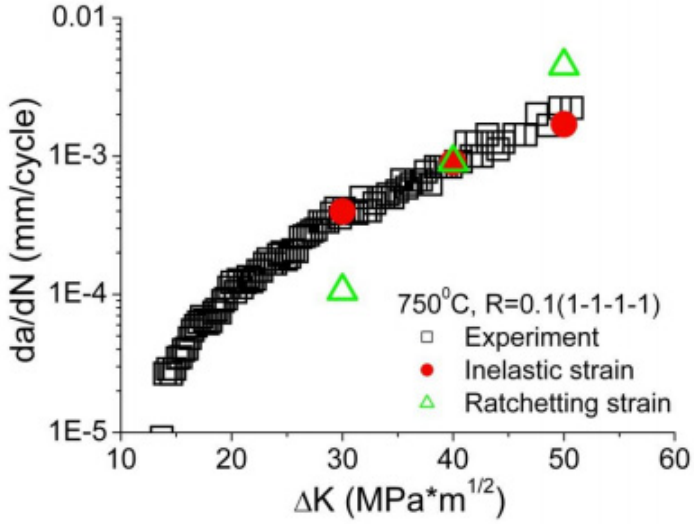

Figure 4(d): Comparison of the results from the experiment and the FE model prediction for crack growth at 750°C (R=0.1; loading waveform 1-1-1-1).

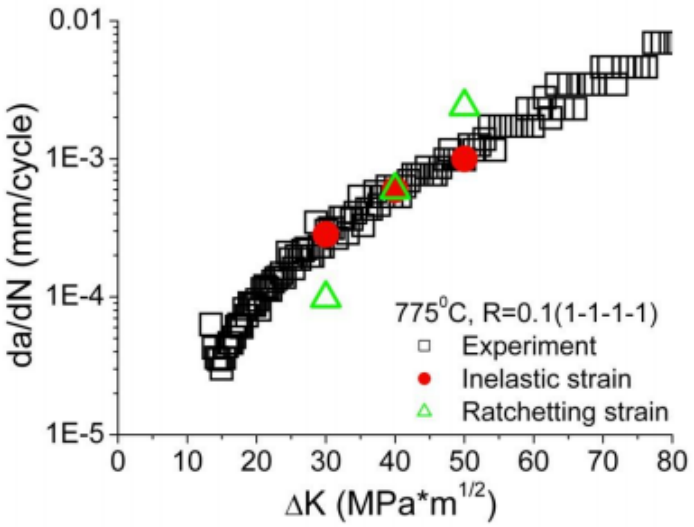

Figure 4(e): Comparison of the results from the experiment and the FE model prediction for crack growth at 775°C (R=0.1; loading waveform 1-1-1-1).

ACCEPTED MANUSCRIPT

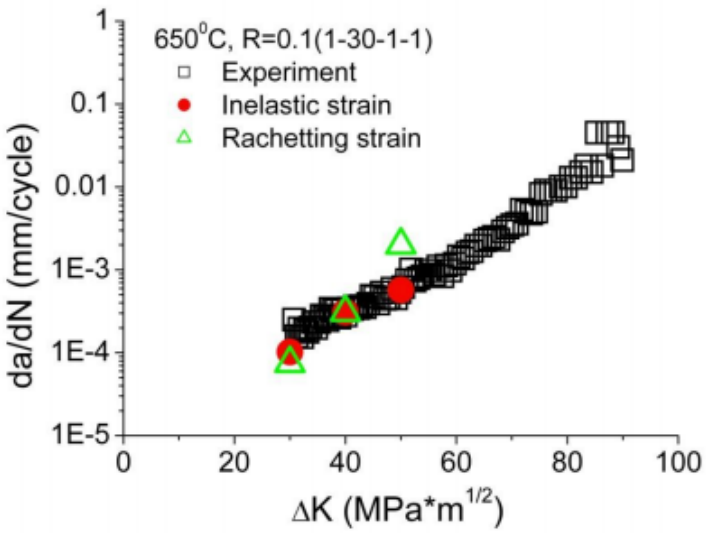

Figure 4(f): Comparison of the results from the experiment and the FE model prediction for crack growth at 650°C (R=0.1; loading waveform 1-30-1-1).

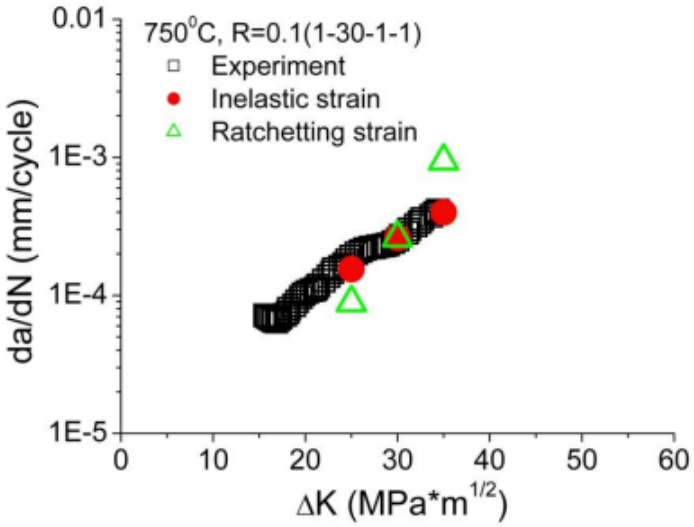

Figure 4(g): Comparison of the results from the experiment and the FE model prediction for crack growth at 750°C (R=0.1; loading waveform 1-30-1-1).

ACCEPTED MANUSCRIPT

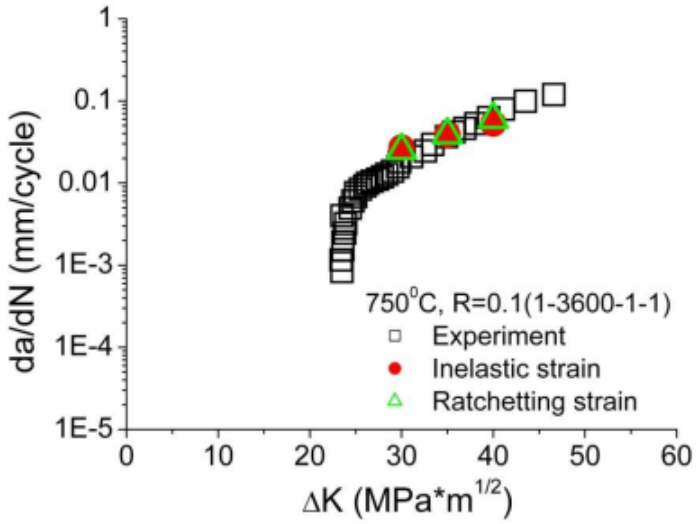

Figure 4(h): Comparison of the results from the experiment and the FE model prediction for crack growth at 750°C (R=0.1; loading waveform 1-3600-1-1).

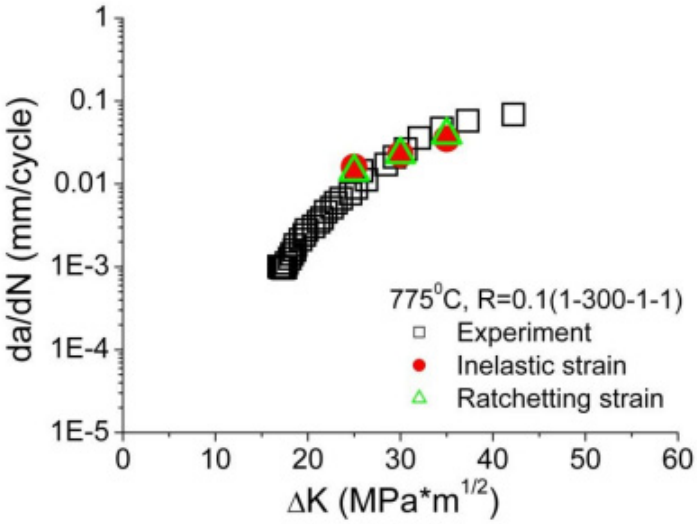

Figure 4(m): Comparison of the results from the experiment and the FE model prediction for crack growth at 775°C (R=0.1; loading waveform 1-300-1-1).

ACCEPTED MANUSCRIPT

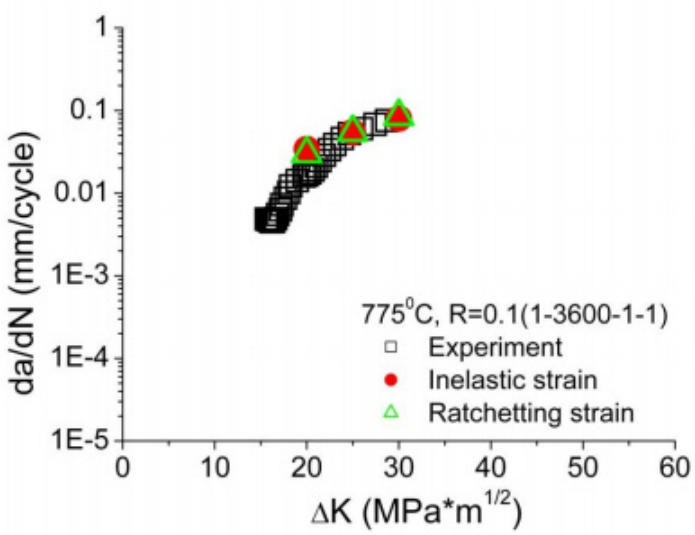

Figure 4(n): Comparison of the results from the experiment and the FE model prediction for crack growth at 775°C (R=0.1; loading waveform 1-3600-1-1).

ACCEPTED MANUSCRIPT

ACCEPTED MANUSCRIPT

Highlights

- Concept of ratchetting strain used to predict fatigue crack growth in vacuum for the first time.
- Accumulated inelastic strain predicts well fatigue crack growth rates of a nickel alloy from 550 to 775C.
- Unified constitutive model used effectively for the prediction of crack growth rates under fatigue and fatigue-creep loading conditions.

ACCEPTED MANUSCRIPT